# 9

# Cloud cover and cloudy-sky radiation parameterizations

## 9.1 Introduction

The amount of sky covered by clouds, or cloud cover, can substantially alter the amount of radiation received at the Earth's surface, thereby influencing atmospheric circulations and climate. Clouds both reflect and absorb shortwave radiation, altering the total albedo. Under overcast skies, the reduction in the incoming shortwave radiation due to the clouds can be substantial. In addition, clouds absorb and emit longwave radiation in the atmospheric window, the wavelength band in which the atmosphere is almost transparent to longwave radiation. The ability of clouds to alter substantially both the shortwave and longwave radiative transfer highlights their importance to numerical weather prediction across a range of spatial and temporal scales.

Small-scale atmospheric circulations develop in response to horizontal differential heating as discussed in Chapter 2. Horizontal variability in cloud cover can lead to surface differential heating and the development of mesoscale thermally induced circulations between cloudy and clear areas (Koch 1984; Segal *et al.* 1986). These circulations can reach magnitudes similar to those associated with sea breezes with the potential to aid in both the development of deep convection and frontogenesis across weak or moderate cold fronts (Koch 1984; Keyser 1986; Segal *et al.* 1986, 1993; Businger *et al.* 1991). Segal *et al.* (1986) further argue that even short-lived episodes of cloudy–clear air contrasts can lead to changes in the low-level wind fields. The effects of cloud shading underneath thunderstorm anvils may be important to the evolution of thunderstorms (Markowski and Harrington 2005).

On much longer timescales, clouds play a very important role in the Earth's radiation budget. It is clear that clouds act as a radiative feedback to climate by reflecting the incoming solar radiation, and absorbing and emitting the terrestrial longwave radiation. This feedback is rather complex, with clouds

generally acting to cool the surface except in polar regions where the albedo of cloudy regions can be less than the surface albedo (Schneider 1972). An increase in low- and mid-level clouds leads to cooling, owing to the increase in albedo, while an increase in high-level cirrus clouds leads to warming, owing to the associated increase in longwave absorption and emission without much change to shortwave radiation. The ability of clouds to produce both a positive and a negative climate feedback, owing to the details in the horizontal and vertical cloud characteristics, indicates both the importance and sensitivity of three-dimensional cloud cover treatment for simulations of global climate change (Stephens 2005). Uncertainties in how clouds are parameterized in models are one of the principal obstacles preventing more accurate climate change prediction (Webster and Stephens 1983). Numerous studies have shown that model simulations are sensitive to the specification of cloudiness (e.g., Meleshko and Wetherald 1981; Shukla and Sud 1981).

Cloud cover also can be modified by aerosols. Aerosols from both natural and anthropogenic sources act as condensation nuclei for cloud droplets, such that increases in the amount of aerosol can increase low-level cloud cover (Twomey 1977). However, increases in aerosols also change cloud lifetimes and precipitation efficiencies (Albrecht 1989) and some aerosols produce a reduction in cloud reflectance (Kaufman and Nakajima 1993). Thus, the interrelationships between climate, humans, and clouds are complex and highlight the challenges in global climate simulations.

The largest challenge to cloud cover parameterization is that the formation and dissipation of clouds is, in general, poorly understood. And since clouds are subgrid scale, both horizontally and vertically, there is neither a complete theory nor an observational database that can be used to relate cloud cover to the large-scale variables (Slingo 1987). Yet cloud cover is very important because it has a significant influence on incoming solar radiation and downwelling longwave radiation, not to mention the heating rates from radiative flux divergence in the atmosphere. Eliminating cloud cover in a mesoscale model can easily alter temperatures in the lowest model layer by at least 2 K in winter and 4 K in summer over the central and eastern USA (Cortinas and Stensrud 1995). The effects of cloud cover typically are even larger in desert regions.

It is important to recognize that cloud cover is three-dimensional and can vary in the vertical direction as well as the horizontal. In numerical models, cloud cover is defined as the fraction of a specified vertical column (grid cell) of air that has clouds contained within it when evaluated within selected vertical layers. Some parameterizations evaluate cloud cover over three or four fairly deep vertical layers, roughly corresponding to the depths associated with the

visual groupings of clouds (low, middle, and high clouds). Other parameterizations evaluate the cloud cover for every vertical model level. Values of cloud cover range from 0 for a cloud-free sky to 1 for an overcast sky.

To understand how one might parameterize cloud cover, first consider the physical processes that lead to cloud formation. Typically, clouds occur because of interactions between vertical motions, turbulence, radiation processes, and microphysical processes. Because of the complexity of cloud formation and the lack of a sound theory to describe it, two approaches have been used to attempt to relate cloud cover to other variables (Slingo 1980).

1. A statistical or diagnostic approach, in which cloudiness is predicted empirically from observed or model variables. Note that using rawinsonde data in a statistical approach has typically not been very successful owing to problems with both the representativeness of point measurements from soundings being applied to areas the size of model grid cells and the lack of detailed information on cloud cover as a function of height (Slingo 1980).
2. A prognostic approach, in which the cloud water content has been explicitly calculated using a model. Unfortunately, until recently there has been very little available verification data to determine if the cloud water contents are reasonable and to document the fine-scale structures of the resulting clouds. Observational experiments, such as the Winter Icing and Storms Project (WISP; Rasmussen *et al.* 1992) and the Improvement of Microphysical PaRameterizations through Observational Verification Experiment (IMPROVE; Stoelinga *et al.* 2003), are beginning to fill this need. However, cloud fields are fractal (Cahalan and Joseph 1989), suggesting that some diagnostic element is always needed.

The need for a cloud cover parameterization scheme in a given numerical weather prediction model depends upon both the model grid spacing and the choices of the model user. Clearly, a cloud cover parameterization scheme is needed for grid spacing larger than 10 km, since so many clouds at that resolution are subgrid phenomena. However, as grid spacing decreases it is difficult to determine exactly when one can rely on the model to generate the appropriate clouds directly and at the right time. If the model has a microphysical parameterization scheme that includes cloud water, then certainly the model is capable of developing clouds or pseudo-clouds. However, clouds at times are very small-scale features and the dividing line between needing and not needing a cloud cover parameterization scheme as a function of grid spacing is unclear. For example, Dudhia (1989) assumes a cloud cover of either 0 or 1 for both longwave and shortwave radiation within a numerical model that uses 10 km grid spacing. Is this a wise choice? Condensation processes often occur at scales much smaller than 10 km, and many clouds have a length scale of perhaps several hundred meters. So the answer to the

question is likely to depend upon the phenomena that the user wants to be able to reproduce and the user's sensitivity to errors. Certainly the errors in cloud cover should decrease as the model grid spacing decreases, since fewer and fewer clouds will be subgrid scale, but comparisons between cloud cover produced from very high-resolution model forecasts and from observations have yet to be done. We do not really know how well the smallest grid-spacing models handle clouds over large regions. In addition, it is not clear whether or not cloud cover parameterizations based upon large-scale observations are helpful as the model grid spacing becomes small. Certainly more attention is needed on this issue.

## 9.2 Cloud cover parameterizations

There are two main types of cloud cover parameterizations being used in numerical weather prediction models. The first type is a diagnostic cloud cover parameterization, in which cloud cover is diagnosed after each time step from the model variables and then used to modify the amounts of shortwave and longwave radiation. These parameterizations generally are very simple and computationally inexpensive. The second type is a prognostic cloud cover parameterization, in which cloud cover is added as a predicted model variable along with a second variable for cloud water. These parameterizations are more complicated and also more expensive computationally.

### *9.2.1 Diagnostic cloud cover*

When considering how cloud cover could be statistically related to observed variables, an important consideration is what variables to explore in developing this relationship. Smagorinsky (1960) originally proposed using relative humidity to predict cloud cover, a reasonable first-order relationship. However, the relationship between model-grid-scale cloudiness and relative humidity obviously has complicating factors. While it is clear that relative humidity plays a significant role (Fig. 9.1), as when Slingo (1980) notes that in the absence of a boundary layer inversion, low clouds almost always occurred when the relative humidity exceeded 80%, there also is little doubt that other factors are also important. Thus, most studies have focused upon an examination of relative humidity, convective activity, vertical velocity, stability, wind shear, and surface fluxes. Some of these are clearly surface variables, such as surface fluxes, while others extend throughout the depth of the troposphere or have no specific vertical level assignment, such as convective activity. All of these approaches try to ascertain when clouds form and how much of a given

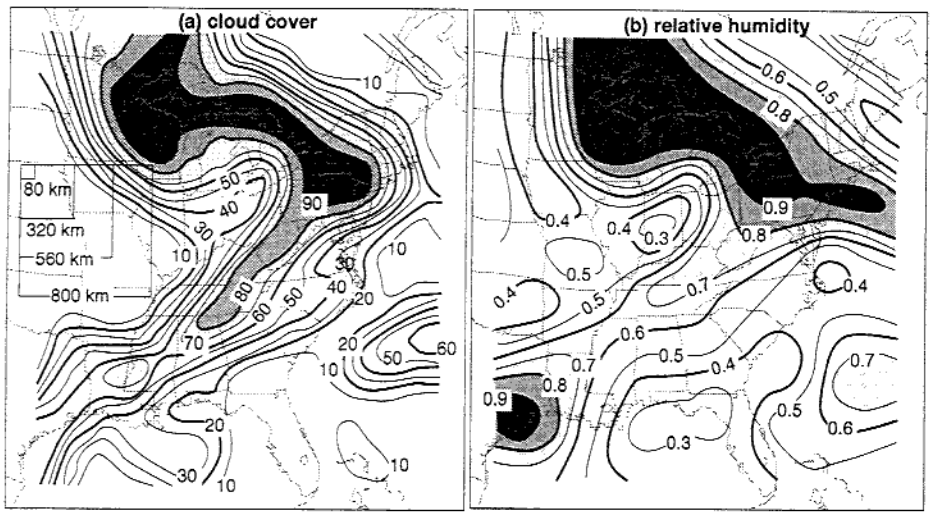


Figure 9.1. Cloud cover (a) and relative humidity (b) averaged over $(320\,\text{km})^2$ areas in the 800–730 hPa layer at 1800 UTC 23 April 1981. Cloud cover is from the United States Air Force three-dimensional cloud analysis scheme, while the relative humidity is from the interpolated observations. Squares in (a) illustrate different horizontal grid spacings. From Walcek (1994).

model grid cell contains cloud at a given time, since subgrid scale fluctuations in temperature and moisture can lead to areas where condensation occurs well before the grid mean values become saturated. While a variety of approaches can be found in the literature, several approaches are surveyed that suggest the basic ideas behind cloud cover parameterization.

The first approach examined is that of Benjamin and Carlson (1986), as also discussed in Anthes *et al.* (1987). In this approach, the cloud fraction ($b$), which varies from 0 to 1, is defined as

$$b = 4.0RH - 3.0, \tag{9.1}$$

for low and middle clouds, and

$$b = 2.5RH - 1.5, \tag{9.2}$$

for high clouds, where $RH$ is the maximum relative humidity found within the model layers associated with each type of cloud. Low clouds are defined as those located below 800 hPa, middle clouds are defined as those between 800 and 450 hPa, and high clouds are those located above 450 hPa. Note that these relationships indicate that no low and middle clouds are found for maximum relative humidities below 75%, and no high clouds are found for maximum relative humidities below 60%. Basically, this scheme provides a linear increase in cloud cover as maximum $RH$ increases past its layer-dependent, predetermined

minimum thresholds. Once the cloud fraction $b$ is calculated, then modifications to both the incoming solar radiation and downwelling longwave radiation due to clouds can be determined.

The second cloudiness approach examined is that of Slingo (1987), which was implemented operationally in the European Centre for Medium-range Weather Forecasting (ECMWF) medium-range forecast model in 1985. One distinct difference between this approach and that of Benjamin and Carlson (1986) is that cloud fraction is calculated for each model level in the Slingo approach, instead of only for three vertical layers in the Benjamin–Carlson approach. Yet the Slingo approach again has three basic types of clouds (low, middle, and high), but adds another level of complexity by including the effects of parameterized deep convection on cloud cover ($b_{conv}$), such that

$$b_{conv} = a + d\ln(P), \tag{9.3}$$

where $P$ is the precipitation rate from the numerical model, and $a$ and $d$ are empirically defined constants. The cloud fraction produced by parameterized convection may be needed in a numerical model, since some convective parameterization schemes produce little if any moistening in the upper levels when they are activated, necessitating a separate parameterization to account for the high-level cloudiness typically observed. Note that $b_{conv} < 0.80$ always.

Slingo (1987) also divides the resulting total cloudiness from $b_{conv}$ into both low-level clouds (75%) and deep tropospheric clouds (25%). For the high- and mid-level clouds created by convective processes, the scheme has for cloud tops above 400 hPa

$$b_{high} = 2.0(b_{conv} - 0.3) \qquad \text{for} \quad b_{conv} > 0.40 \tag{9.4}$$

and for cloud tops below 400 hPa it has

$$b_{mid} = 0.25 b_{conv}. \tag{9.5}$$

The model convective scheme provides information on the cloud base and the cloud top, and also the precipitation rate $P$ needed to define $b_{conv}$.

The Slingo scheme also computes the cloud fraction based only upon the $RH$ of each model layer, such that for extratropical and frontal cirrus clouds

$$b_{high} = \left[\max\left\{0, \frac{(RH - 0.8)}{0.2}\right\}\right]^2 \tag{9.6}$$

and

$$b_{mid} = \left[\max\left\{0, \frac{(RH_e - 0.8)}{0.2}\right\}\right]^2, \tag{9.7}$$

where $RH_e = RH\ (1.0 - b_{conv})$ and it attempts to account for the so-called compensating subsidence from deep convection in the mid-levels. This scheme uses the same pressure levels to define low, middle, and high clouds as Benjamin and Carlson (1986) discussed previously.

Low-level clouds are the most troublesome to handle, since these are very dependent upon the surface fluxes and model boundary layer structures. Observational studies suggest that low-level clouds depend upon a delicate balance between cloud-top entrainment, radiative cooling, and surface fluxes. All of these factors are difficult for a model to predict accurately. In this scheme, $b_{low}$ is divided into contributions associated with extratropical cyclones and tropical disturbances, and associated with boundary layer processes. The portion attributed to cyclones and tropical disturbances is predicted by the relationships

$$\hat{b}_{low} = \left[\max\left\{0, \frac{(RH_e - 0.8)}{0.2}\right\}\right]^2 \qquad \text{if} \quad \omega < 0, \tag{9.8}$$

where $\omega$ is the model vertical velocity in pressure coordinates. When subsidence is indicated ($\omega \geq 0$), then

$$b_{low} = 0.0. \tag{9.9}$$

The actual diagnosed low-level cloud cover $b_{low}$ depends directly upon $\hat{b}_{low}$, such that

$$b_{low} = \hat{b}_{low}(-10.0\omega), \tag{9.10}$$

for $\omega < -0.1$ Pa s$^{-1}$. Therefore, there is a linear relationship between the amount of cloud cover diagnosed and the model-predicted vertical motion fields.

For boundary layer clouds, the low-level cloud cover depends upon the low-level lapse rate such that

$$b_{low} = -6.67\frac{\Delta\theta}{\Delta p} - 0.667, \tag{9.11}$$

where $\Delta\theta/\Delta p$ is the lapse rate in the most stable layer below 750 hPa. An extra check is also added to make certain that the $RH$ is high enough to develop clouds (i.e., no clouds are diagnosed when the air is dry).

This approach is based upon an examination of the available observational studies of cloud cover as related to various observed parameters, and an in-depth analysis of the ECMWF model output and comparisons against observed cloud cover. While very empirical in nature, this approach includes a great deal of complexity in relating the model variables to cloud development.

The third scheme is from the United States National Centers for Environmental Prediction Eta Model and follows Sundqvist (1988). This scheme also calculates cloud cover for each model level, and again has three basic types of clouds. However, the pressure levels that distinguish the three layers are somewhat different from the previous two schemes. In the Eta model, the cloud cover ($b$) for low ($p > 800$ hPa), middle (400 hPa $< p <$ 800 hPa), and high ($p < 400$ hPa) clouds is given by

$$b = 1.0 - \left[\frac{(1.0 - RH)}{(1.0 - RH_{crit})}\right]^{1/2}, \tag{9.12}$$

where $b = 0$ when $RH < RH_{crit}$ and

$$RH_{crit} = RH1 + F1(L)(0.95 - RH1)F2(t), \tag{9.13}$$

with $L$ defined as the model level number above the ground surface. The variable $RH1$ equals 0.8 over water and equals 0.75 over land. The function $F1(L)$ varies linearly from 1 to 0 in the first ten layers above the ground. Thus, $F1(1) = 1.0$, $F1(2) = 0.9$, $F1(3) = 0.8$, and so forth, up to $F1(11) = 0.0$. This sequencing obviously causes $F1$ to increase towards the surface of the model, and causes $RH_{crit}$ similarly to increase. Thus, it requires a larger value of $RH$ to form clouds at the very lowest model levels. The function $F2(t)$ varies linearly from 0 to 1 in the first 24 h of the forecast and is fixed at 1 after hour 24. The maximum value of $RH$ found in each layer is used to calculate the cloud cover.

When these three schemes are compared for low clouds at 800 hPa, it is seen that the Benjamin–Carlson scheme predicts less cloud cover than either the Slingo or Eta schemes for all relative humidity values less than 100% (Fig. 9.2). Additionally, the Slingo and Eta schemes are very similar in their shape, although the exact values for the Slingo scheme depend somewhat on the magnitude of the vertical motion. All of these types of diagnostic approaches are designed for a particular model at a particular model grid spacing, so one must be cautious when applying these schemes to other models and at other values of grid spacing. The basic relationship between relative humidity and cloud cover likely remains a reasonable first-order approximation, but the parameterization details (such as the threshold relative humidity at which clouds first begin to form) may need to be altered.

### 9.2.2 *Prognostic cloud cover*

Many numerical models include explicit microphysics parameterizations as discussed in Chapter 7. Depending upon the complexity of these schemes, the model may contain equations for cloud water, rain water, cloud ice, and snow,

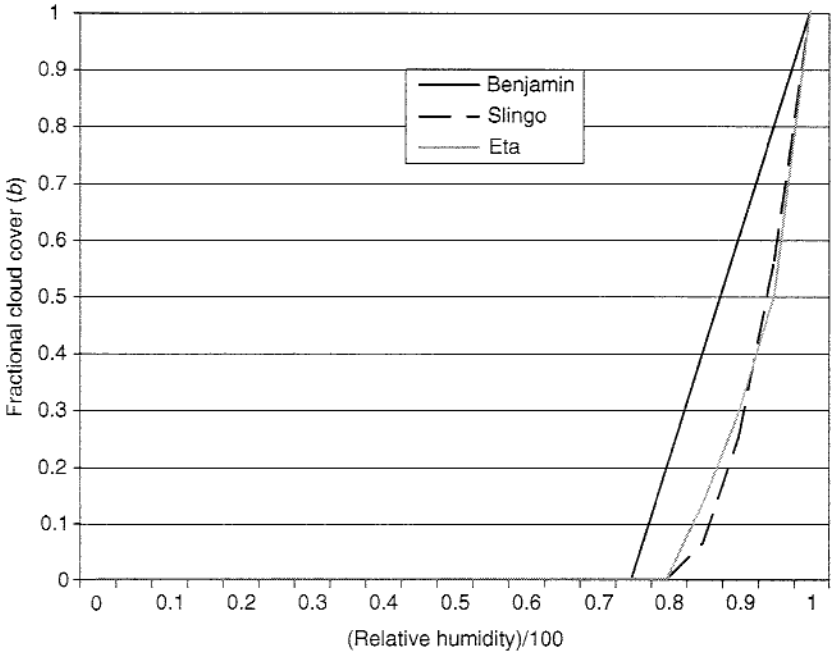


Figure 9.2. Value of cloud cover versus relative humidity scaled from 0 to 1 from the Benjamin–Carlson (solid black), Slingo (dashed), and Eta model (solid gray) cloud cover schemes for low clouds at 800 hPa. The Slingo and Eta schemes have very similar profiles as a function of relative humidity.

and perhaps even graupel and hail. When models predict these explicit cloud variables, it is important that there is consistency between the explicitly predicted cloud variables and the cloud cover parameterization often used to feed needed information to the radiation parameterization. It is possible that the model-produced cloud water or cloud ice may not be consistent with the cloud cover diagnosed and used by the radiation parameterization (Sundqvist *et al.* 1989), a situation one would prefer to avoid.

For cloud-scale models and some mesoscale models with sophisticated microphysical parameterization schemes and relative small grid spacing, a binary cloud cover can be deduced directly from the cloud water fields that the model predicts. In these cases, cloud cover is either explicitly 1 or 0, depending upon whether or not cloud water is present in a given grid cell. Typically in this case the cloud fraction is not diagnosed and there is no cloud cover parameterization; instead the predicted cloud water is used directly in the calculations for the radiative fluxes. It is important to emphasize again that there are no subgrid scale clouds in this approach. As mentioned previously, the grid spacing for which this type of approach is appropriate is likely to be less than 10 km, and may

be smaller than 2 km, but needs to be determined by the user and depends upon the type of clouds the model needs to represent. For small cumulus clouds a grid spacing of a hundred meters may be needed before this type of approach is valid.

For models that use larger grid spacings, and in which cloud development needs to occur prior to grid-scale saturation, another approach is desired that allows for partial cloudiness within the grid cell. The first example of a fully prognostic approach to the parameterization of fractional cloud cover is from Sundqvist (1988) and is extended by Sundqvist *et al.* (1989). This cloud cover parameterization scheme only requires an additional predictive equation for cloud water ($q_c$), and so avoids the large number of additional equations required in many of the more sophisticated microphysics schemes discussed in Chapter 7. Thus, this type of scheme is much more computationally efficient than a complete microphysics parameterization, and yet contains parameterizations of many of the same physical processes – albeit at an even more simplified level.

These approaches begin by assuming that within each grid cell there are cloudy areas and cloud-free areas (Sundqvist 1988). Thus, the relative humidity $U$ of the grid cell is a weighted average of the humidity in the cloudy area, $U_S \equiv 1$, and the humidity in the cloud-free area, $U_0$, such that

$$U = bU_S + (1 - b)U_0, \tag{9.14}$$

where $b$ is the cloud cover and varies from 0 to 1 as before. Sundqvist *et al.* (1989) further assume that the humidity of the cloud-free area depends upon both the amount of cloud cover and a basic threshold humidity $U_{00}$ that is allowed to vary as a function of model level and temperature. These assumptions lead to the expression

$$U_0 = U_{00} + b(U_S - U_{00}), \tag{9.15}$$

for the humidity in the cloud-free area. Finally, combining (9.14) and (9.15) yields a diagnostic equation for cloud cover in terms of $U$ and $U_{00}$, such that

$$b = 1 - \left(\frac{U_S - U}{U_S - U_{00}}\right)^{1/2}, \tag{9.16}$$

allowing cloud cover to be determined from the evolution of the grid cell relative humidity $U$ and noting that $b = 0$ for $U < U_{00}$. This equation expresses the same relationship between relative humidity and cloud cover as used by the Eta model as described in (9.12).

The prognostic cloud cover approach hinges upon an expression for the grid-resolved latent heating rate ($Q$) due to condensation derived by Sundqvist (1988). Beginning with the relationship

$$q = Uq_s, \tag{9.17}$$

where $q_s$ is the saturation specific humidity and taking the derivative with respect to time, one finds

$$\frac{\partial q}{\partial t} = \frac{\partial U}{\partial t} q_s + U \frac{\partial q_s}{\partial t}. \tag{9.18}$$

Using the approximation $q_s \cong \varepsilon e_s / p$ to replace $q_s$ in the last term of (9.18), where $e_s$ is the saturation vapor pressure, $p$ is pressure, and $\varepsilon = 0.622$, yields

$$\frac{\partial q}{\partial t} = \frac{\partial U}{\partial t} q_s + \frac{U\varepsilon}{p} \frac{\partial e_s}{\partial t} - \frac{U\varepsilon e_s}{p^2} \frac{\partial p}{\partial t}. \tag{9.19}$$

Making use of the Clausius–Clapeyron equation, $de_s/dT = \varepsilon L_v e_s / R_d T^2$, where $R_d$ is the specific gas constant for dry air, and $L_v$ is the latent heat of vaporization, some further manipulation leads to an expression for the specific humidity tendency in terms of the tendencies of temperature, humidity, and pressure,

$$\frac{1}{q} \frac{\partial q}{\partial t} = \frac{\varepsilon L_v}{R_d T^2} \frac{\partial T}{\partial t} + \frac{1}{U} \frac{\partial U}{\partial t} - \frac{1}{p} \frac{\partial p}{\partial t}. \tag{9.20}$$

Following Sundqvist *et al.* (1989), the tendency equations for temperature, specific humidity, and the cloud water mixing ratio ($q_c$) in the case of stratiform condensation and evaporation are

$$\frac{\partial T}{\partial t} = A_T + \frac{L_v}{c_p} Q - \frac{L_v}{c_p} E_0, \tag{9.21}$$

$$\frac{\partial q}{\partial t} = A_q - Q + E_0, \tag{9.22}$$

$$\frac{\partial q_c}{\partial t} = A_{q_c} + Q - (P - E_r) - E_0, \tag{9.23}$$

where the $A$-terms represent the tendencies due to all processes other than condensation and evaporation, $c_p$ is the specific heat of air at constant pressure, $P$ is the rate of release of precipitation, $E_r$ is the evaporation rate of precipitation, and $E_0$ is the total evaporation rate due to $E_r$ and the evaporation of cloud water. When the environment is saturated, $U \equiv 1$ and the second term on the right-hand side of (9.20) is identically zero. If this modified version of (9.20) for saturated conditions is inserted into (9.22), and if (9.21) is then used to eliminate the temperature tendency, one arrives at

$$Q = \frac{M - q_s(\partial U / \partial t)}{1 + U\varepsilon L_v^2 q_s / R_d c_p T^2} + E_0, \tag{9.24}$$

where $M$ is the convergence of available latent heat into the grid cell. The convergence term $M$ is defined as

$$M = A_q - \frac{U\varepsilon L_v q_s}{R_d T^2} A_T + \frac{U q_s}{p} \frac{\partial p}{\partial t}. \tag{9.25}$$

The system of equations is closed by providing an expression for the $U$-tendency. Sundqvist *et al.* (1989) assume that the quantity $M + E_0$ can be divided into two parts. One part, $bM$, condenses in the cloudy portion of the grid cell, while the other part, $(1-b)M + E_0$, increases the relative humidity of the cloud-free portion and hence the cloud cover of the grid cell. This assumption leads to the tendency equation

$$\frac{\partial U}{\partial t} = \frac{2(1-b)(U_S - U_{00})[(1-b)M + E_0]}{2q_s(1-b)(U_S - U_{00}) + q_c/b}. \tag{9.26}$$

Since the latent heating rate $Q$ is incorporated into the $T$, $q$, and $q_c$ tendency equations (9.21)–(9.23), there is a direct link between changes in cloud cover and the model tendency equations.

Since cloud cover is incorporated into the model predictive equations, it also should be incorporated into any other relevant parameterizations. For example, Sundqvist *et al.* (1989) define the autoconversion from cloud water to precipitation as

$$P_{AUTO} = c_0 q_c \left[ 1 - \exp\left[ -\left( \frac{q_c}{b q_{c\_threshold}} \right)^2 \right] \right], \tag{9.27}$$

where $c_0$ and $q_{c\_threshold}$ are constants ($c_0 = 1.0 \times 10^{-4}$ s$^{-1}$ and $q_{c\_threshold} = 3.0 \times 10^{-4}$ in Zhao and Carr (1997)). Note how the cloud cover $b$ appearing in the exponential influences the autoconversion rate, allowing for larger autoconversion rates for smaller values of cloud cover as $q_c$ is held constant. It is the cloud water content per cloud area that is seen to determine the rate at which precipitation is produced.

The evaporation of precipitation also depends upon the cloud cover as well as the relative humidity of the grid cell (Sundqvist *et al.* 1989). The total evaporation rate $E_0$ is calculated from both the evaporation of precipitation and the evaporation of cloud water that occurs when cloud water is advected into a grid cell where no condensation is taking place. In addition, a direct link between the convective parameterization scheme and the creation of cloud water is created as part of the scheme (Sundqvist *et al.* 1989). Thus, the effects of cloud cover are accounted for in all the appropriate terms in the model equations, allowing for consistency between the microphysics and cloud cover.

While Sundqvist *et al.* (1989) further include simple representations of the coalescence process, the Bergeron–Findeisen mechanism, and the microphysical properties of cirrus clouds, Zhao and Carr (1997) extend this parameterization to include cloud ice processes. The inclusion of cloud ice processes led to significant improvements in the Eta model precipitation forecasts (Zhao and Carr 1997). This type of approach is also implemented and tested by Pudykiewicz *et al.* (1992).

The prognostic representation of cloud cover is further extended by Tiedtke (1993) through the development of tendency equations for both cloud water content and cloud cover. Thus, cloud cover is a predicted variable in the numerical model just like temperature and specific humidity. For example, it is assumed that the formation of cloud water is determined by the decrease in the saturation specific humidity. In addition, condensation is assumed to occur in both existing clouds (if any) and in new clouds, leading to

$$\frac{\partial q_c}{\partial t_{cond}} = -b\frac{dq_s}{dt} - \Delta b\frac{dq_s}{dt}, \qquad \frac{dq_s}{dt} < 0, \tag{9.28}$$

where *cond* refers to the tendency from processes associated with condensation only, and $\Delta b$ is the fractional cloud cover increase per time step. If moisture is distributed evenly around the mean environmental value of specific humidity, then Tiedtke (1993) finds that the change in cloud cover is given by

$$\frac{\partial b}{\partial t_{cond}} = -(1-b)\frac{dq_s/dt}{(q_s - q)}, \qquad \frac{dq_s}{dt} < 0, \tag{9.29}$$

thereby indicating how decreases in the saturation specific humidity cause both an increase in cloud water and an increase in cloud cover. Parameterizations are also developed for the processes of evaporation, precipitation, and turbulence, and are incorporated into both the cloud water and cloud cover equations as in (9.28) and (9.29). This approach allows for cloud-related processes to be treated uniformly. The scheme further links the grid-scale variables to the convective scheme, such that the formation of cloud due to cumulus convection is tied to the detrainment of cloud mass in the updraft of the convective parameterization scheme. Tests of this scheme within the ECMWF global forecast model indicate that realistic cloud fields are produced (Tiedtke 1993). Other examples of this type of approach for mesoscale models are found in Ballard *et al.* (1991) and Bechtold *et al.* (1993), and for global climate models are found in Le Treut and Li (1991), Del Genio *et al.* (1996), Fowler *et al.* (1996), and Teixeira and Hogan (2002).

There also exists a group of schemes that often are called "statistical schemes" in which a probability density function is assigned to the total water mixing ratio

(the sum of the water vapor and all liquid and ice mixing ratios) and, by defining the statistical moments of the distribution of the total water mixing ratio, one can diagnose the cloud fraction by integrating the supersaturated portion of the probability density function. Examples of these schemes are found in Smith (1990), Cusack *et al.* (1999), Lohmann *et al.* (1999), Bony and Emanuel (2001), Chaboureau and Bechtold (2002), Thompkins (2002), and Berg and Stull (2005). The Smith (1990) scheme is extended by Wilson and Ballard (1999) to include cloud ice processes. These schemes incorporate estimates of subgrid scale variability into the diagnosis of the cloud cover fraction, but still do not predict cloud cover explicitly. Chaboureau and Bechtold (2002) show that the partial cloudiness scheme reduces the biases in the shortwave and infrared spectral ranges in comparison to explicit microphysical schemes without partial cloudiness, yielding better agreement with synthetic satellite imagery.

Finally, yet another prognostic cloud cover scheme is suggested by Grabowski and Smolarkiewicz (1999) and Grabowski (2001) in which a cloud-resolving model is run within the grid cell of a model with much larger grid spacing. This scheme is called a "superparameterization" by Randall *et al.* (2003). While this approach is typically viewed as an alternative for global climate models, the approach also may be reasonable for some operational forecast models for the treatment of cumulus clouds. The basic idea is to embed a two-dimensional cloud-resolving model within the grid cell of a model that does not explicitly simulate clouds (Fig. 9.3) and to use the cloud-resolving model output to compute statistics for fractional cloudiness, cloud water, and precipitation rate for the larger-scale model's grid column. Initial results suggest that the global model simulations with this superparameterization are able to produce a vigorous Madden–Julian Oscillation (MJO), in contrast with the control run with a typical cloud parameterization

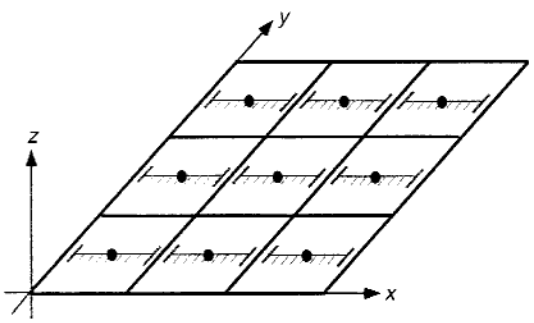


Figure 9.3. Schematic of a superparameterization of cloud effects, in which the black squares represent the large-scale model grid cells and the hatched lines represent a two-dimensional cloud-resolving model domain within each large-scale model grid cell. From Randall *et al.* (2003).

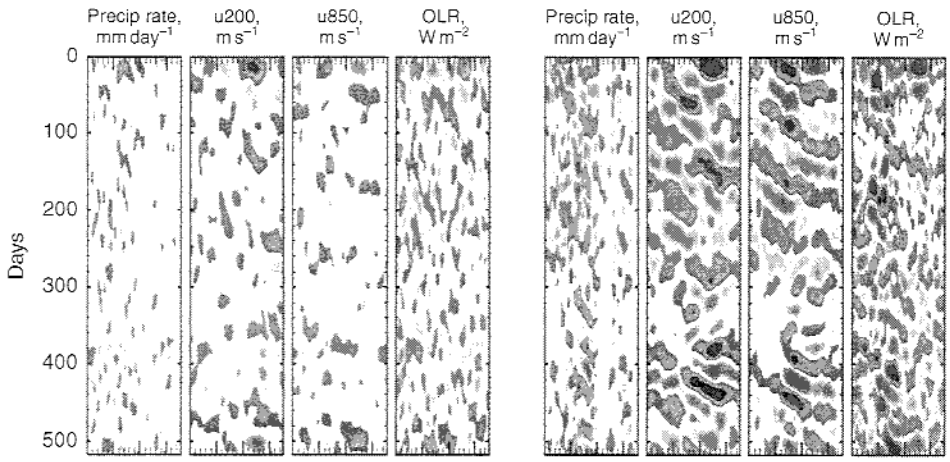


Figure 9.4. Hovmöller diagrams for the precipitation rate (mm day$^{-1}$), 200 hPa zonal wind (m s$^{-1}$), 850 hPa zonal wind (m s$^{-1}$), and outgoing longwave radiation (OLR, W m$^{-2}$) for wave periods of 20–100 days from the same global model with (left) a traditional cloud cover and convective parameterization approach and (right) a superparameterization that embeds a cloud-resolving model into each grid cell of the larger-scale model. Each subpanel spans 0° to 360° in longitude at a tropical latitude. Note that the superparameterization results indicate a vigorous Madden–Julian oscillation (illustrated by the coherent patterns) that is completely absent from the simulation with a traditional cloud cover parameterization. From Randall *et al.* (2003).

scheme that essentially has no MJO (Fig. 9.4). Although computationally much more expensive than a more traditional cloud-cover approach, the superparameterization approach is much cheaper than a full cloud-resolving model simulation and represents an interesting use of a combination of models developed for simulating different scales of atmospheric phenomena.

## 9.3 Cloud–radiation interactions

Now that the cloud fractions are diagnosed in the model, or cloud water is present, the question turns to how these fields feed back into the shortwave and longwave radiation predicted at the surface and at various model levels. As before, the longwave and shortwave parameterization schemes are discussed separately.

### *9.3.1 Longwave radiation in cloudy skies*

Longwave heating rates within clouds are typically calculated by assuming that the clouds radiate as blackbodies. Stephens (1978a) shows that a cumulonimbus

cloud with a liquid water content of 2.5 g m$^{-3}$ radiates as a blackbody beyond a depth of 12 m into the cloud. In contrast, a thin stratus cloud with a liquid water content of 0.05 g m$^{-3}$ radiates as a blackbody only beyond a depth of 600 m into the cloud, which may be more than the vertical grid increment of many of the models in use today. Cirrus clouds are probably the most difficult, because of the relatively low level of water content present in these clouds and their importance to climate (Liou 1986; Stephens *et al.* 1990). Liou and Wittman (1979) suggest that cirrus clouds should be considered gray bodies instead. Thankfully, the dominance of liquid water absorption over scattering by cloud droplets simplifies the problem and allows for the development of relatively simple approximations. This is not necessarily true for cirrus clouds when ice is present.

Stephens (1978b) shows that longwave radiative flux is most sensitive to the cloud water path (*CWP*), and this has been found to be true regardless of whether the cloud is composed of cloud droplets or ice crystals. The effects of rain and snow on longwave flux are two to three orders of magnitude less than the effects of cloud water and ice. This result suggests that rain and snow can be neglected to first order in quantifying the longwave radiation in cloudy skies, although approaches have been developed to incorporate the effects of rain and snow.

If the model being used has cloud water and cloud ice as predicted variables, owing to the use of a microphysical parameterization, then it is very easy to calculate the *CWP*. This is simply the integral

$$CWP = \int_{z_1}^{z_2} w \, dz, \tag{9.30}$$

where $z_1$ and $z_2$ are the heights over which the *CWP* needs to be determined, and $w$ is the cloud liquid water content in g m$^{-3}$. However, if a numerical model does not include cloud water as a variable, determination of a *CWP* is still required to parameterize the radiative effects of subgrid scale clouds. Kiehl *et al.* (1996) prescribe a meridionally and height varying, but time-independent, cloud liquid water density profile $\rho_l(z)$ that is analytically determined. This profile represents an exponentially decaying vertical profile for in-cloud water concentration, such that

$$\rho_l(z) = \rho_{l0} e^{-z/h_l}. \tag{9.31}$$

where the reference value $\rho_{l0}$ is set to 0.21 g m$^{-3}$. The cloud water scale height $h_l$ is locally determined as a function of the vertically integrated water vapor. Thus, the *CWP* can be calculated even for models without explicit microphysical schemes and used in the longwave flux calculations for cloudy skies. Now

that the $CWP$ is available for the model, we turn to how the interactions between clouds and radiation occur. Much of the following discussion is based upon Stephens (1978b) and Dudhia (1989).

When dealing with the interactions between clouds and radiation, the total cloud emissivity, which can be calculated from the measurement of the longwave radiative flux profile through the cloud and the cloud temperature, is the appropriate parameter to use (Stephens 1978b). The emissivities of very different cloud types are nearly identical if their $CWP$ is the same. Cloud emissivity is calculated using

$$\varepsilon_{cloud} = 1 - e^{a_0 CWP}, \tag{9.32}$$

where $a_0 = 0.158$ for downward longwave flux and $a_0 = 0.130$ for upward longwave flux. These two different values are found because the spectral compositions of the upward and downward beams incident on the cloud boundaries are so different. This total cloud emissivity is actually an "effective" emissivity, since it includes the combined effects of absorption and scattering.

Since the cloud total emissivity applies across the entire infrared spectrum, the problem of having cloud and gaseous absorption occurring in the same spectral band must be addressed. This is often accounted for using the overlap approximation, in which

$$\varepsilon_{total} = 1 - (1 - \varepsilon_{cloud})(1 - \varepsilon_{gas}), \tag{9.33}$$

where $\varepsilon_{gas}$ can be for water vapor or another gas such as $CO_2$.

For ice clouds, Dudhia (1989) uses the same general approach as for cloud water, but specifies $a_0 = 0.0735\,\mathrm{m^2\,g^{-1}}$, a value of roughly half that for water vapor. Dudhia also develops an emissivity equation for rain and snow that can be combined with the cloud and gas emissivities using the overlap approximation.

Once the emissivities are known for each atmospheric layer in the model, the addition of clouds adds extra boundaries to the clear-sky longwave radiative flux calculations. As shown by Stephens (1978b), the flux equations above and below a cloud with cloud top height $z_T$ and cloud base height $z_b$ are

$$F_U(z) = \sigma T^4(z_T)[1 - \varepsilon(z, z_T)] + \int_{z_T}^{z} \sigma T^4(z') \frac{d\varepsilon(z, z')}{dz'}\, dz' \qquad z > z_T, \tag{9.34}$$

and

$$F_D(z) = \sigma T^4(z_b)[1 - \varepsilon(z_b, z)] + \int_{z_b}^{z} \sigma T^4(z') \frac{d\varepsilon(z, z')}{dz'}\, dz' \qquad z < z_b. \tag{9.35}$$

Fluxes within the cloud are defined by interposing $z_T$ and $z_b$ and by specifying the appropriate cloud emissivity.

Another approach is developed by Savijärvi and Räisänen (1998) in which the longwave radiation parameterization is based upon the $CWP$ and the effective cloud droplet radius. In models with explicit microphysics schemes, the effective cloud droplet radius $r_e$ can be calculated explicitly from

$$r_e = \frac{\int_0^\infty n(r) r^3 \, dr}{\int_0^\infty n(r) r^2 \, dr}, \tag{9.36}$$

where $r$ is the droplet radius, and $n(r)$ is the droplet size distribution function. If the numerical models do not include an explicit microphysical parameterization, then Savijärvi and Räisänen (1998) provide an estimate for $r_e$ based upon the $CWP$ that depends upon whether the clouds are maritime or continental.

When ice is present in the cloud, then the cloud particles are not necessarily spherical as assumed for cloud droplets. This alters the calculations of the scattering and absorption coefficients and the asymmetry factor. Ebert and Curry (1992) and Fu *et al.* (1998) parameterize the optical properties of ice crystal clouds. Ebert and Curry (1992) use the ice water path and an effective ice crystal radius to describe the ice optical properties. They find that a change in the effective ice crystal radius alone is more effective than a change in just the ice water path in altering shortwave reflectivity and the cloud albedo feedback. Fu *et al.* (1998) use observations of 28 ice crystal distributions to relate the width of a crystal to its length and parameterize the absorbtivity, reflectivity, and transmissivity using both the ice water content and the generalized effective particle size.

Another challenge arises when a given cloud layer is only partially filled with cloud. Since models with explicit microphysics are capable of resolving clouds to some extent, these models generally assume either an entirely clear or an entirely cloudy grid cell. Thus, partially cloudy layers typically occur in models with diagnostic cloud cover schemes and convective parameterization schemes. In this case the longwave flux is determined by linearly weighting the clear-sky and cloud-sky fractions, such that

$$F_U(z) = (1 - b) F_{U_{clear}}(z) + b F_{U_{cloud}}(z), \tag{9.37}$$

where $b$ is the cloud fraction. Harshvardham and Weinman (1982) demonstrate that this linear weighting is reasonable if the model-derived cloud fraction is replaced with

$$b' = \frac{[1 + 2a(1 + 0.15b)]b}{1 + 2ab(1 + 0.15b)}, \tag{9.38}$$

where $a$ is the aspect ratio (depth over width) of the cloud. This result is based upon a study of black square blocks, which approximate clouds, over a radiating surface, and takes into account some of the three-dimensional effects of broken clouds.

While there are a number of other details and complexities that could be addressed, the last one to be discussed here is the problem of cloud vertical overlap in models that use a cloud cover parameterization. Most of these models diagnose cloud cover for each vertical model layer, and these values of fractional cloud cover vary with height. The concern is how the cloud cover fractions from adjacent layers are related to each other. As shown earlier, partially cloudy skies are divided into sectors in which the amount of cloud is either 0 or 1 and they are then linearly weighted to determine the resulting longwave flux. When adjacent layers both have clouds, there are two common approaches to determine how these adjacent cloud fractions are related. One approach is to assume that the cloud fractions randomly overlap (Manabe and Strickler 1964). This approach defines the amount of sky covered simultaneously by $n$ layers by the relationship

$$1-(1-b_1)(1-b_2)(1-b_3)\cdots(1-b_n), \tag{9.39}$$

where $b_1$ to $b_n$ are the cloud fractions of the $n$ layers. This approach assumes that clouds are distributed randomly in each layer and that the clouds in one layer are not necessarily related to the clouds in an adjacent layer. An alternative approach is a maximum/random overlap method (Geleyn and Hollingsworth 1979), where the cloud fraction from a combination of layers is given by the maximum cloud fraction determined at any one layer which is overlapped and any excess cloud is positioned randomly across the layer. This latter approach is suggested by the work of Tian and Curry (1989) to be more consistent with the distribution of observed clouds. Stephens *et al.* (2004) compare the most common cloud vertical overlap assumptions and find that two methods, the random and maximum-random overlap methods, have severe problems since they depend upon the vertical resolution of the numerical model.

It is clear that the problem of cloud–radiation interactions is a difficult and challenging one. The parameterizations examined are relatively complex, but the atmosphere is even more so. The cloud–radiation and feedback problem is one that has been highlighted as a crucial area where more work is needed in order to be able to better address global climate change and it definitely influences short-range operational weather prediction as well.

### 9.3.2 Shortwave radiation in cloudy skies

As with longwave radiative flux in cloudy skies, the shortwave radiative flux depends mostly on the cloud water path. The heart of the problem is to determine realistic values for the cloud optical properties of optical thickness $\tau$, single-scattering albedo $\tilde{\omega}_0$, and asymmetry factor $g$. Of these properties, the optical thickness is the most important parameter. Stephens (1978b) suggests that a rough range for optical thickness is between 5 and 500. Twomey (1976) notes that if the sun's disk is not visible through a cloud layer, then the optical thickness must be equal to 10 or more. The absorption of shortwave radiation by cloud droplets cannot be neglected when compared against the absorption by water vapor and needs to be included in many models.

Stephens (1978b) provides a derivation that outlines the various steps in determining the cloud optical thickness $\tau$. When all is said and done, the result is simply that

$$\tau \approx \frac{3}{2}\frac{CWP}{r_e}, \tag{9.40}$$

where $r_e$ is the effective drop size from (9.36). This parameterization is based upon a specified set of calculations using eight cloud types (Stephens 1978b). Values of cloud optical thickness typically range from 1 to 500.

Further simplifications can be made by noting that liquid water absorption in clouds only occurs for $\lambda > 0.75\,\mu\text{m}$. Thus, Stephens separates the solar spectrum into two parts: 0.3–0.75 μm for which no absorption occurs and the single-scattering albedo $\tilde{\omega}_0 = 1$, and 0.75–4.0 μm for which absorption occurs and $\tilde{\omega}_0 < 1$. Scattering occurs in both of these parts of the solar spectrum. He then derives expressions for the broad-band optical thickness of cloud layers as a function of $CWP$ only, with

$$\log_{10}(\tau) = 0.2633 + 1.7095 \log_e[\log_{10}(CWP)] \qquad \tilde{\omega}_0 = 1 \tag{9.41}$$

and

$$\log_{10}(\tau) = 0.3492 + 1.6518 \log_e[\log_{10}(CWP)] \qquad \tilde{\omega}_0 < 1. \tag{9.42}$$

He notes that the effective radius of a cloud droplet distribution is intuitively a function of liquid water content, and hence by extension $CWP$. Thus, we should not be surprised that the effective radius can be removed from these relationships.

Following Coakley and Chylek (1975), the reflection ($Re$) and transmission ($Tr$) through a cloud layer of optical thickness $\tau$ as defined in (9.41) and (9.42) is given by

$$Re(\mu_0) = \frac{\beta(\mu_0)\tau/\mu_0}{1 + \beta(\mu_0)\tau/\mu_0}, \tag{9.43}$$

$$Tr(\mu_0) = 1 - Re(\mu_0), \tag{9.44}$$

for a non-absorbing medium with $\tilde{\omega}_0 = 1$, and

$$Re(\mu_0) = (u^2 - 1)\left[\exp(\tau_{eff}) - \exp(-\tau_{eff})\right]/R, \tag{9.45}$$

$$Tr(\mu_0) = 4u/R, \tag{9.46}$$

for an absorbing medium with $\tilde{\omega}_0 < 1$ and where

$$u^2 = [1 - \tilde{\omega}_0 + 2\beta(\mu_0)\tilde{\omega}_0]/(1 - \tilde{\omega}_0), \tag{9.47}$$

$$\tau_{eff} = \{(1 - \tilde{\omega}_0)[1 - \tilde{\omega}_0 + 2\beta(\mu_0)\tilde{\omega}_0]\}^{1/2}\tau/\mu_0, \tag{9.48}$$

and

$$R = (u + 1)^2 \exp(\tau_{eff}) - (u - 1)^2 \exp(-\tau_{eff}). \tag{9.49}$$

Here $\beta$ is the backscattered fraction of monodirectional incident radiation at the zenith angle $\mu_0$. Stephens (1978b) tuned values of $\tilde{\omega}_0$ to match the flux values provided by more accurate numerical solutions and provides a lookup table such that one can obtain $\tilde{\omega}_0$ given the values of $\tau$ and $\mu_0$. This approach similarly removes the dependence of $\tilde{\omega}_0$ on the effective cloud droplet radius, and is used by Dudhia (1989) among others. Thus, the gross shortwave radiative effects of clouds can be determined largely from the values of *CWP* and zenith angle.

A problem arises in that water vapor and cloud droplet absorption overlap, yet behave quite differently. As Stephens (1984) discusses, the absorption by liquid water is a smooth function of wavelength, whereas the absorption by water vapor varies strongly with wavelength. A method for calculating the absorption for cloudy skies that overlaps the cloud droplet and molecular absorptions is needed. Stephens discusses several options that are available.

Owing to the importance of high-level cirrus clouds to climate, Ebert and Curry (1992) and Fu (1996) develop ice cloud parameterization schemes. The single-scattering properties of solar radiation are parameterized in terms of the ice water path and the generalized effective particle size in both schemes.

When model layers are only partially cloudy, then various weightings between the clear-sky and cloudy-sky fractions are often used, as is done for longwave radiation and discussed previously. These weightings include minimum

cloud overlap, maximum cloud overlap, random overlap, maximum-random overlap, and variations on linear weightings. Stephens *et al.* (2004) suggest that the maximum-random and random overlap methods depend upon the vertical resolution of the numerical model and thereby suffer severe problems. Welch *et al.* (1980) suggest that radiative transfer through the three-dimensional cloud shapes is not quite as simple as one might hope and that linear weightings are an oversimplification. The development of improved parameterizations for model-relative partial cloud (in the horizontal and vertical directions) is clearly needed.

## 9.4 Discussion

The parameterization of cloud cover is yet another important component in many numerical weather prediction models. While the need for this type of parameterization may indeed decrease and perhaps vanish as model grid spacings become smaller and smaller, observations suggest that even at 2 km grid spacing clouds can occur as a subgrid phenomenon. And for global models, the need for cloud cover parameterization is going to continue for some time until computers become fast enough for cloud-resolving models to be run at global scales.

We have seen that there exist a wide variety of approaches that attempt to deal with diagnosing or predicting cloud cover, ranging from simple relationships between relative humidity and cloud cover to fully prognostic schemes that include the cloud fraction as a model variable and integrate this variable with other model parameterization schemes. Comparisons between observations of relative humidity and cloud cover indicate a large scatter (Fig. 9.5). Walcek (1994) shows that, within the 800 to 730 hPa layer, at 80% relative humidity there is a nearly uniform probability of observing any cloud fraction. The standard deviation of cloud cover approaches 40% within restricted relative humidity ranges using an 80 km grid cell (Fig. 9.5c). One interpretation of these results is that the cloud cover is influenced by much more than relative humidity, which is certainly true. Another interpretation is that our ability to correctly predict cloud cover is limited, since cloud cover parameterizations based upon relative humidity are competitive with more sophisticated schemes as indicated by their continued use in operational forecast models.

Similarly, Hinkelman *et al.* (1999) compare the Eta model liquid or ice mixing ratio with observations at the Atmospheric Radiation Measurement Southern Great Plains site in Oklahoma during the first half of 1997. Their results suggest that the Eta model, in general, produces a reasonable mean representation of explicit clouds when compared against the cloud radar

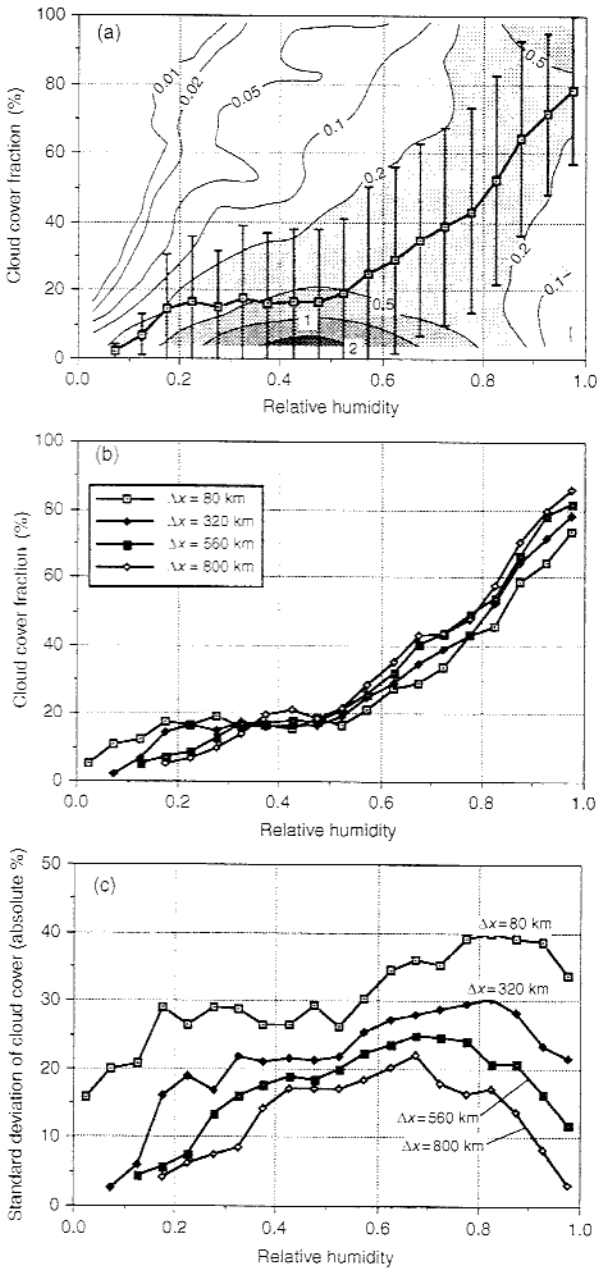


Figure 9.5. (a) A joint frequency distribution showing the probability (%) of observing various cloud cover and relative humidity combinations averaged over $(320\ \text{km})^2$ areas in the 800–730 hPa layer from five local noon samples. The solid dark curve with error bars shows the mean and standard deviation of cloud cover. (b) The mean cloud cover as a function of relative humidity in the 800–730 hPa layer for various averaging areas. (c) The standard deviation of the cloud cover within restricted relative humidity ranges for various area sizes. From Walcek (1994).

reflectivity data. There is a mean overprediction of cirrus events in the Eta model during the first 3 months of the year and a mean underprediction of mid-level clouds in the springtime. Zhou and Cess (2000) show that the diagnosed cloud heights play a large role in the surface energy budget. Differences in the downwelling longwave radiation of 31 $W m^{-2}$ are found when cloud heights are shifted upwards 2 km and downwards 2 km for mid-level clouds. High clouds have a smaller influence on the longwave radiation since they are cooler than the mid-level clouds. Thus, not only do we need to predict cloud cover and cloud water content accurately, but the cloud base and the cloud top as well. Barker *et al.* (2003) compare results from numerous solar radiation parameterizations with observations and conclude that none of the schemes do well under all cloud cover conditions.

Part of the problem in predicting cloud cover is that the observational data set for cloud cover has a number of uncertainties, including the differences in the perspectives of the data sets. Clouds can be observed above a point using ceilometer measurements for cloud base heights of up to ~3600 m, cloud cover can be estimated visually by surface and aircraft observers, and the cloud top and the cloud fraction can be estimated from satellite data (Schreiner *et al.* 1993). Buriez *et al.* (1988) and Chang and Coakley (1993) find that different methods of diagnosing the cloud cover fraction from satellite imagery yield differences of 16–30%, which is very similar to the standard deviations of cloud cover when compared to relative humidity measurements (Fig. 9.5c). In contrast to the observations, cloud cover in a numerical model is determined for a specific horizontal area and height that change as the model grid spacing changes. Applying the satellite cloud amount to models requires the use of a cloud overlap assumption, and Zhou and Cess (2000) indicate that the use of different overlap assumptions can produce differences in the incoming surface longwave radiation of 20 $W m^{-2}$. They conclude that more information on cloud overlap and more accurate cloud profiling are needed. Thus, uncertainties in the observed cloud fractions are likely to contribute to the difficulty in developing good parameterizations for cloud cover.

However, even assuming there exists a near-perfect parameterization for the cloud cover fraction, challenges still exist in calculating the absorption of shortwave and longwave radiation by clouds. Stephens and Tsay (1990) summarize the disagreements between the theoretical and observed values of both cloud absorption and reflection of solar radiation. They show that a number of studies have measured the mean atmospheric absorption by clouds to be as high as 15–40%, whereas theoretical values are typically in the 5–10% range for the cloud types considered. One possible explanation for this disagreement is the effect of cloud heterogeneity on cloud absorption and reflection,

although no clear explanation to account for the discrepancy between observation and theory has emerged.

Another challenge that has emerged is the importance of the cloud microphysics variables to cloud–radiation interactions. Results from a single-column model suggest that the effective cloud droplet radius influences the model radiative fluxes (Iacobellis and Somerville 2000). Similarly, Liu *et al.* (2003) show that the assumed ice crystal habits can have a significant influence on the evolution of cirrus clouds and, therefore, on both the solar and infrared radiative heating rates for these clouds. Results from Gu and Liou (2000) indicate that the model simulated ice crystal size distribution within cirrus clouds depends strongly on the simulated radiative heating profiles. Within mesoscale convective systems, the strength of the rear inflow jet is influenced by the interactions between longwave cooling and ice microphysics (Chen and Cotton 1988). Yet it is not at all clear that the radiation and microphysics parameterization schemes in most models have identical specifications for the effective cloud droplet radius or ice crystal size distributions and also are able to pass this information from one parameterization to the other as needed.

Since the magnitudes of downwelling longwave radiation are not as large as the incoming solar radiation, errors in this parameterization may have a smaller influence on the model forecast accuracy. However, errors in cloud representation can lead to non-trivial differences in the downwelling radiation (Fig. 9.6) that may influence local predictions. In addition, cloud geometry effects play a role in longwave scattering under broken cloudiness conditions (Takara and Ellingson 2000), further complicating the situation.

As mentioned in the previous chapter, if the instantaneous values of observed and predicted surface shortwave or longwave radiation are examined, large differences are seen (e.g., Fig. 9.6). Many if not all of these larger differences are due to clouds passing over the observation site, which obviously are not accurately predicted by the numerical model. It may be that these differences, which often persist for relatively short periods of time, do not matter and the model forecasts do not suffer from these inaccuracies. But it also may be true that under some situations these differences do matter and result in unexpected consequences, such as the initiation of deep convection from growing thermals. Thus, the way one views the accuracy of parameterizations in general depends upon what types of events are important and what processes influence these events. It remains an open question as to how important these differences are to accurate and useful numerical weather prediction.

Finally, three-dimensional effects can be very important for radiation–cloud interactions. All the one-dimensional radiative transfer parameterizations discussed are challenged in cloudy atmospheres and as the horizontal grid

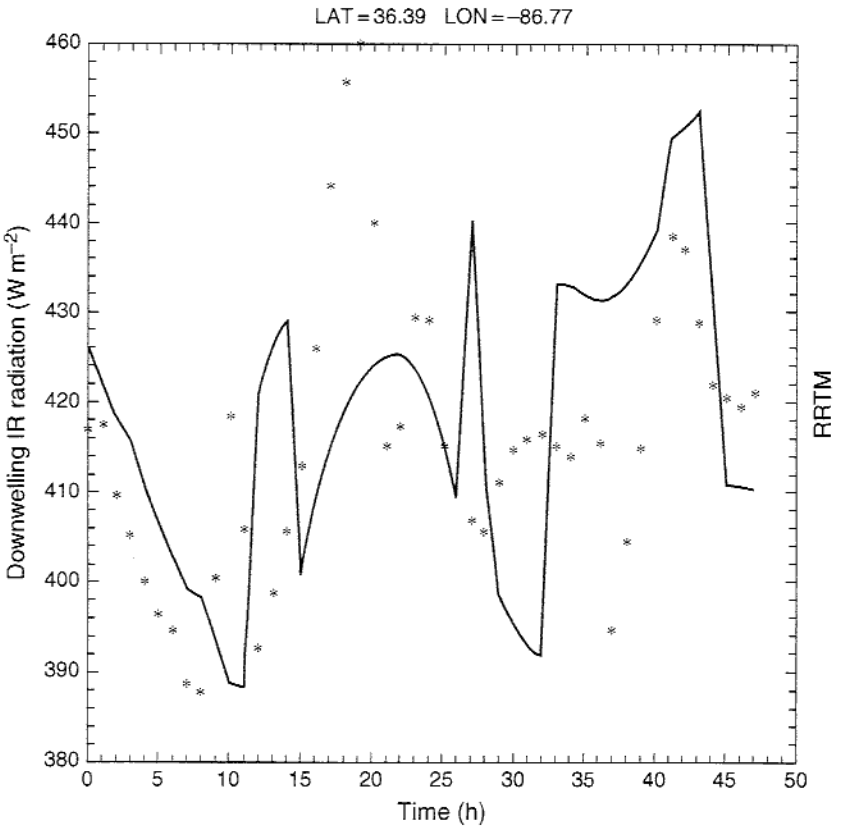


Figure 9.6. Downwelling infrared radiative flux predicted by the RRTM (solid line) from a mesoscale model simulation and measured (asterisks) at Cornelia Fort Airpark, Tennessee, as a function of time for 3–4 July 1995. From Zamora *et al.* (2003).

spacing in the model decreases, making the plane-parallel assumption dubious. The transfer of photons between different parts of a cloud or between neighboring grid cells cannot be accounted for in one-dimensional radiative transfer parameterizations. Unfortunately, while three-dimensional radiative transfer approaches have been developed, they are not yet affordable for use in operational models (Marshak and Davis 2005; Cahalan *et al.* 2005).

## 9.5 Questions

1. Fill in the details in the derivation of the Sundqvist cloud cover parameterization approach. Starting with (9.17) derive (9.24).
2. Let us examine the effects of clouds on longwave radiation. Assume a very simple atmosphere with only one layer, with $F_{Dclear} = 315\,\mathrm{W\,m^{-2}}$ and $F_{Dcloud} = 350\,\mathrm{W\,m^{-2}}$.

Using (9.37) and (9.38), calculate the downwelling surface longwave radiation as a function of cloud cover. Also vary the cloud aspect ratio from 1 to 5. Describe the results.

3. Using the results of Question 2, how large are the errors in the downwelling surface radiation for uncertainties of 30% in the cloud cover? What does this say about the importance of cloud cover parameterization in models?
4. Turning our attention to shortwave radiation, vary the values of the cloud water path from 10 to 10 000 g m$^{-2}$ and calculate the transmissivity using (9.42). Assuming that the incoming shortwave radiation at the top of the cloud is 800 W m$^{-2}$, plot the values of shortwave radiation exiting the bottom of the cloud as a function of the cloud water path using (9.43)–(9.49). Assume that $\mu_0 = 0.87$, $\beta = 0.06$, and $\tilde{\omega}_0 = 0.8$.
5. Using the results of Question 4 with a cloud water path of 1000 g m$^{-2}$, determine the difference in the shortwave radiation exiting the bottom of the cloud for an uncertainty of 100 g m$^{-2}$ in the cloud water path. Since cumulonimbus clouds are associated with cloud water paths of 10 000 g m$^{-2}$, an error of 10% or 1000 g m$^{-2}$ is probably even more reasonable for this cloud type. Repeat the difference calculations for the exiting shortwave radiation at the bottom of the cumulonimbus cloud. How important are these uncertainties to the resulting calculations of shortwave radiation?